

Possible deformation evolution in the $\pi i_{13/2}$ structure of ^{171}Re

D. J. Hartley,¹ E. E. Pedicini,^{1,*} R. V. F. Janssens,² L. L. Riedinger,³ M. A. Riley,⁴ X. Wang,⁴ S. Miller,⁴ A. D. Ayangeakaa,^{5,†} M. P. Carpenter,² J. J. Carroll,⁶ J. Cavey,¹ C. J. Chiara,^{2,7,8} P. Chowdhury,⁹ U. Garg,⁵ S. S. Hota,^{9,‡} E. G. Jackson,⁹ F. G. Kondev,¹⁰ T. Lauritsen,² M. Litz,⁶ W. C. Ma,¹¹ J. Matta,⁵ E. S. Paul,¹² J. Simpson,¹³ J. R. Vanhoy,¹ and S. Zhu²

¹*Department of Physics, U.S. Naval Academy, Annapolis, Maryland 21402, USA*

²*Physics Division, Argonne National Laboratory, Argonne, Illinois 60439, USA*

³*Department of Physics and Astronomy, University of Tennessee, Knoxville, Tennessee 37996, USA*

⁴*Department of Physics, Florida State University, Tallahassee, Florida 32306, USA*

⁵*Department of Physics, University of Notre Dame, Notre Dame, Indiana 46556, USA*

⁶*Army Research Laboratory, Adelphi, Maryland 20783, USA*

⁷*Department of Chemistry and Biochemistry, University of Maryland, College Park, Maryland 20742, USA*

⁸*Nuclear Engineering Division, Argonne National Laboratory, Argonne, Illinois, 60439, USA*

⁹*Department of Physics, University of Massachusetts Lowell, Lowell, Massachusetts 01854, USA*

¹⁰*Nuclear Engineering Division, Argonne National Laboratory, Argonne, Illinois 60439, USA*

¹¹*Department of Physics, Mississippi State University, Mississippi State, Mississippi 39762, USA*

¹²*Oliver Lodge Laboratory, University of Liverpool, Liverpool L69 7ZE, United Kingdom*

¹³*STFC Daresbury Laboratory, Daresbury, Warrington WA4 4AD, United Kingdom*

(Received 27 August 2013; published 21 October 2013)

The phenomenon of wobbling can only occur for a nuclear shape with stable triaxial deformation. To date, only a few examples of this exotic collective mode have been observed in lutetium and tantalum isotopes. A search for a wobbling sequence was performed in ^{171}Re to determine if this feature can be observed in $Z > 73$ nuclei. No evidence was found for wobbling; however, an interaction between the $\pi i_{13/2}$ sequence and another positive-parity band may give an indication on why wobbling may not occur in this nucleus. The level scheme for ^{171}Re was significantly extended and interpretations for the decay sequences are proposed within the context of the cranked shell model.

DOI: [10.1103/PhysRevC.88.044323](https://doi.org/10.1103/PhysRevC.88.044323)

PACS number(s): 21.10.Re, 23.20.Lv, 27.70.+q

I. INTRODUCTION

The region of nuclei with $Z \approx 72$ and $N \approx 94$ has drawn interest over the past decade with the observation of wobbling excitations in several lutetium nuclei [1–4] and most recently in ^{167}Ta [5,6]. This collective wobbling motion can only occur when the nucleus possesses a stable triaxial shape, which has proven to be one of the most challenging shapes to confirm experimentally. In this region, an enhanced quadrupole deformation is required in order to stabilize a gap in the orbitals near the Fermi surface that favors the formulation of an asymmetric shape [7]. Therefore, all the wobbling bands in the lutetium and tantalum isotopes have been based on the deformation-driving $i_{13/2}$ quasiproton. In order to determine whether wobbling exists beyond the $Z = 73$ tantalum nuclei, an experiment was performed to populate high-spin states in ^{171}Re such that a search for this rather elusive collective mode could be conducted.

Unfortunately, no evidence for wobbling in ^{171}Re was found. It will be shown that an interaction between the $\pi i_{13/2}$

band and another positive-parity sequence may provide a possible explanation for the lack of wobbling in this nucleus. However, the level scheme was greatly extended to higher spin and six new decay sequences were observed. More than 175 new γ -ray transitions have been added to the previously known level scheme [8,9]. Configuration assignments are proposed based on their observed alignments, $B(M1)/B(E2)$ ratios, and other rotational band characteristics. In addition to the interaction found with the $\pi i_{13/2}$ structure, a Landau-Zener crossing is observed between the $\alpha = +1/2$ signatures of the $\pi h_{11/2}$ and $\pi h_{9/2}$ sequences.

II. EXPERIMENTAL DETAILS

The experiment was conducted at the ATLAS facility at Argonne National Laboratory and the Gammasphere array [10] detected the emitted γ rays. A beam of ^{55}Mn was accelerated to an energy of 257 MeV and directed onto two, stacked targets of isotopically enriched ^{120}Sn . One target had a thickness of approximately $500 \mu\text{g}/\text{cm}^2$, the other $\sim 700 \mu\text{g}/\text{cm}^2$. A beam current of ~ 2.5 pA was sustained through the three days of beam time, and over 2.0×10^9 threefold, or higher, coincidence events were collected. One hundred detectors were operating in Gammasphere during this experiment.

The data were sorted into a Blue database [11] for the creation of Radware [12] cubes and hypercubes. In addition, an angular-correlation analysis was performed with the Blue database. A sort in the database was conducted for two

*Department of Nuclear Engineering, Texas A & M University, College Station, TX 77843.

†Physics Division, Argonne National Laboratory, Argonne, Illinois 60439.

‡Department of Nuclear Physics, R.S.P.E., Australian National University, Canberra, A.C.T. 0200, Australia.

TABLE I. Measured γ -ray properties in ^{171}Re .

$I\pi^a$	E_{level} (keV)	E_γ (keV) ^b	I_γ ^c	Ang.-corr. ratio
Band 1: [514]9/2 $\alpha = +1/2$				
9^-	0.0			
13^-	380.9	380.9	$\sim 19^d$	0.81(8)
		223.8	$\sim 108^d$	0.81(3)
17^-	894.3	513.4	44(3)	0.84(4)
		279.9	82(5)	0.77(5) ^e
21^-	1474.3	580.0	56(3)	0.92(4) ^e
		311.9	54(3)	0.82(5) ^e
25^-	2072.2	597.9	52(3)	0.87(4) ^e
		314.2	42(2)	0.82(5) ^e
29^-	2546.0	473.8	27(2)	1.06(5)
		202.3	62(3)	0.71(3)
33^-	2889.2	343.2	13(1)	1.0(1)
		184.3	55(3)	0.64(3)
37^-	3355.0	466.0	18(1)	0.82(7)
		248.3	48(2)	0.63(3)
41^-	3937.6	582.6	25(2)	0.92(4) ^e
		301.4	31(2)	0.76(5)
45^-	4606.1	668.4	17(1)	1.01(8)
		339.3	22(1)	0.78(5)
49^-	5330.8	724.7	12.5(6)	1.1(1)
		362.9	13(1)	0.79(4) ^e
53^-	6092.5	761.7	9.3(5)	0.9(1)
		376.0	5.9(6)	0.8(1)
		723.9	2.2(1)	1.1(2)
57^-	6889.0	796.5	5.2(3)	
		381.7	1.0(1)	
		775.1	1.6(2)	1.2(1)
61^-	7725.6	836.6	3.2(3)	
65^-	8611.7	886.1	2.0(1)	
69^-	9554.9	943.2	1.1(1)	
73^-	10553.2	998.3	0.5(1)	
77^-	11592.1	1038.9	<0.5	
81^-	12632	1040	<0.5	
85^-	13698	1066	<0.5	
Band 1: [514]9/2 $\alpha = -1/2$				
11^-	157.1	157.1	$\sim 92^f$	0.70(2) ^e
15^-	614.4	457.4	55(3)	0.83(5)
		233.5	93(5)	0.79(3)
19^-	1162.4	548.0	63(3)	0.99(4)
		268.1	66(3)	0.76(3)
23^-	1758.0	595.5	67(4)	0.87(4) ^e
		283.6	54(3)	0.78(2)
27^-	2343.6	585.6	67(4)	1.06(3)
		271.5	49(3)	0.76(2)
31^-	2704.9	361.3	4.8(5)	
		158.9	48(4)	0.70(2) ^e
35^-	3106.7	401.7	12(1)	1.1(1)
		217.5	54(2)	0.64(3)
39^-	3636.1	529.3	17(1)	1.2(1)
		281.1	37(2)	0.77(5) ^e
43^-	4266.8	630.7	20(1)	1.3(1)
		329.2	25(2)	0.63(4)
47^-	4967.9	701.2	15(1)	1.2(1)
		361.7	14(1)	0.79(4) ^e
51^-	5716.5	748.6	11.1(7)	1.3(2)
		385.7	10.0(6)	0.68(7)

TABLE I. (Continued.)

$I\pi^a$	E_{level} (keV)	E_γ (keV) ^b	I_γ ^c	Ang.-corr. ratio
55^-	6507.3	790.8	5.4(3)	
		414.7	3.8(2)	
		393.3	0.6(1)	
59^-	7351.4	844.1	2.4(1)	
		462.2	<0.5	
		430.4	0.7(1)	
63^-	8262.1	910.7	0.8(1)	
		464.6	0.5(1)	
67^-	9238.4	976.3	0.5(1)	
71^-	10229	991	<0.5	
Band 2: [541]1/2 $\alpha = +1/2$				
5^-	189.6			
9^-	285.0	95.4	$\approx 20^f$	0.69(7)
		127.8	0.7(1)	
13^-	514.1	229.1	93(5)	0.81(2)
17^-	868.8	354.8	$\equiv 100$	0.91(2)
21^-	1326.2	457.4	86(4)	0.97(2)
25^-	1861.7	535.5	77(4)	1.01(3)
29^-	2444.9	583.2	71(3)	1.16(3)
33^-	3007.6	562.7	50(3)	1.21(4)
37^-	3518.8	511.2	41(2)	0.90(4)
41^-	4069.3	550.5	30(2)	1.05(3)
45^-	4686.0	616.7	23(1)	1.13(5)
49^-	5368.9	682.9	14.4(7)	1.06(5)
53^-	6114.2	745.3	9.5(6)	0.97(5)
		397.6	1.4(7)	
		783.3	1.1(6)	
57^-	6921.5	807.3	2.7(8)	1.14(9)
		414.0	1.3(6)	
		(829)	<0.5	
61^-	7797.7	876.2	1.8(1)	
		446.1	0.8(1)	
65^-	8748.2	950.5	<0.5	
69^-	9755	1007	<0.5	
Band 2: [541]1/2 $\alpha = -1/2$				
3^-	301.1	107.9	<0.5	
		110.9	<0.5	
7^-	447.6	146.5	1.4(1)	
		162.1	<0.5	
11^-	700.6	258.0	3.5(2)	0.8(1)
		253.0	6.6(4)	0.68(7)
		186.8	<0.5	
		415.5	4.9(3)	0.9(1)
15^-	1064.9	364.3	7.9(4)	0.94(8)
		550.8	2.2(1)	0.3(1)
19^-	1521.6	456.7	6.9(4)	0.88(4)
		652.8	1.8(1)	0.3(1)
23^-	2043.3	521.7	7.1(4)	1.2(1)
		717.2	1.0(3)	0.34(6) ^e
27^-	2578.9	535.6	7.9(8)	0.92(6) ^e
		717.4	1.3(3)	0.34(6) ^e
31^-	3007.9	429.0	7.5(7)	1.00(5) ^e
		562.9	0.8(1)	
35^-	3458.4	450.5	8.3(8)	0.73(4) ^e
		428.9	2.3(3)	1.00(5) ^e
		450.9	4.4(5)	0.37(4)
39^-	3958.7	500.3	15(1)	1.02(5)
		439.9	3.1(2)	0.44(5)

TABLE I. (Continued.)

TABLE I. (Continued.)

I^π ^a	E_{level} (keV)	E_γ (keV) ^b	I_γ ^c	Ang.-corr. ratio
$\frac{43}{2}^-$	4543.4	584.7	17(3)	0.95(8)
$\frac{47}{2}^-$	5203.6	660.2	11.4(5)	1.1(1)
$\frac{51}{2}^-$	5924.8	721.2	7.1(4)	1.11(8)
$\frac{55}{2}^-$	6698.2	773.4	5.0(3)	1.01(7)
$\frac{59}{2}^-$	7524.8	826.6	3.3(2)	1.06(9)
$\frac{63}{2}^-$	8408.9	884.1	1.8(1)	0.84(9)
$\frac{67}{2}^-$	9370.7	961.8	0.5(1)	
$\frac{71}{2}^-$	10372.4	1001.7	<0.5	
$\frac{75}{2}^-$	11407	1035	<0.5	
		Band 3		
$(\frac{33}{2}^-)$	3262.0	817.1	3.0(2)	1.8(3)
$(\frac{37}{2}^-)$	3892.0	630.0	2.0(1)	
		884.5	1.8(1)	1.5(2)
$(\frac{41}{2}^-)$	4585.4	693.4	1.7(1)	
$(\frac{45}{2}^-)$	5270.0	684.6	1.4(1)	
$(\frac{49}{2}^-)$	5974.3	704.3	1.0(1)	
$(\frac{53}{2}^-)$	6743.0	768.7	0.5(1)	
		Band 4		
$\frac{39}{2}^+$	4222.0	703.4	2.0(1)	0.53(6)
$\frac{43}{2}^+$	4804.3	582.3	<0.5	
		735.0	2.3(2)	0.54(4)
$\frac{47}{2}^+$	5480.3	676.0	0.5(1)	
		794.1	1.4(1)	0.4(1)
$\frac{51}{2}^+$	6225.5	745.2	<0.5	
		856.6	0.9(1)	
$\frac{55}{2}^+$	7050.4	824.9	<0.5	
		936.2	<0.5	
$(\frac{59}{2}^+)$	(7926)	(876)	<0.5	
		Band 5: $\pi h_{11/2}AFBC \alpha = +1/2$		
$(\frac{45}{2}^+)$	5084.7	272.5	1.1(1)	
		280.4	0.8(1)	
$(\frac{49}{2}^+)$	5703.0	618.2	0.9(1)	
		322.3	1.0(1)	
$(\frac{53}{2}^+)$	6404.1	701.0	0.9(1)	
		361.6	0.6(1)	
$(\frac{57}{2}^+)$	7164.6	760.6	0.6(1)	
		389.1	<0.5	
$(\frac{61}{2}^+)$	7974.6	811.0	<0.5	
		413.7	<0.5	
$(\frac{65}{2}^+)$	8846	870	<0.5	
		446	<0.5	
		Band 5: $\pi h_{11/2}AFBC \alpha = -1/2$		
$(\frac{43}{2}^+)$	4812.2	590.3	0.6(1)	
		742.9	1.5(1)	
$(\frac{47}{2}^+)$	5380.6	568.5	0.6(1)	
		295.9	1.3(1)	
		576.5	<0.5	
$(\frac{51}{2}^+)$	6042.5	662.1	0.8(1)	
		339.4	0.8(1)	
$(\frac{55}{2}^+)$	6775.5	733.0	0.5(1)	
		371.3	<0.5	
$(\frac{59}{2}^+)$	7561.7	786.2	0.6(1)	
		397.2	<0.5	
$(\frac{63}{2}^+)$	8400	838	<0.5	
		424	<0.5	
		Band 6: $[402]5/2 \alpha = +1/2$		
$\frac{5}{2}^+$	231.7			

I^π ^a	E_{level} (keV)	E_γ (keV) ^b	I_γ ^c	Ang.-corr. ratio
$\frac{9}{2}^+$	553.5	321.9	$\approx 21^d$	0.73(4) ^e
		171.6	56(3)	0.71(2)
$\frac{13}{2}^+$	960.9	407.3	45(4)	0.95(5)
		202.9	49(5)	0.73(2) ^e
$\frac{17}{2}^+$	1393.1	432.2	45(2)	0.81(4)
		207.3	26(3)	0.75(4)
$\frac{21}{2}^+$	1864.4	471.3	22(2)	0.94(2)
		233.1	12.5(9)	
$\frac{25}{2}^+$	2228.4	123.7	10(1)	0.67(5)
$\frac{29}{2}^+$	2592.4	364.0	4.5(8)	0.8(1)
		200.8	19(2)	0.83(4)
$\frac{33}{2}^+$	3096.2	503.8	12.4(7)	0.96(6)
		266.2	18(1)	0.79(3) ^e
$\frac{37}{2}^+$	3698.2	602.0	14.5(9)	
		311.8	11.0(6)	
$\frac{41}{2}^+$	4340.0	641.7	10.6(6)	
		323.7	8.7(8)	0.73(4) ^e
$\frac{45}{2}^+$	4896.5	556.5	8.8(8)	1.1(1) ^e
		266.1	6.9(4)	0.79(3) ^e
$\frac{49}{2}^+$	5472.7	576.3	3.5(2)	
		300.1	5.9(3)	0.9(1)
$\frac{53}{2}^+$	6159.5	686.8	3.9(2)	
		357.3	4.1(2)	0.6(1)
$\frac{57}{2}^+$	6966.7	807.2	1.2(1)	
		418.8	1.1(1)	
		732.5	1.6(1)	0.90(4)
$\frac{61}{2}^+$	7851.0	884.3	0.5(1)	
		900.4	0.5(1)	
$\frac{65}{2}^+$	8794	943	<0.5	
		Band 6: $[402]5/2 \alpha = -1/2$		
$\frac{7}{2}^+$	381.9	150.2	$\approx 57^f$	0.76(3)
$\frac{11}{2}^+$	758.0	376.2	32(2)	0.69(3)
		204.5	56(6)	0.73(2) ^e
$\frac{15}{2}^+$	1185.9	427.9	41(3)	0.89(5)
		225.0	39(2)	0.70(4)
$\frac{19}{2}^+$	1631.3	445.4	28(3)	0.99(9)
		238.1	23(1)	0.80(4) ^e
$\frac{23}{2}^+$	2104.7	473.4	48(5)	0.90(7)
		240.3	10.7(8)	0.80(4) ^e
		400.3	1.7(2)	
$\frac{27}{2}^+$	2391.6	163.2	22(1)	0.68(3)
$\frac{31}{2}^+$	2829.9	438.4	6.0(3)	0.83(7)
		237.5	17(2)	0.77(4)
$\frac{35}{2}^+$	3386.4	556.5	8.2(6)	1.1(1) ^e
		290.2	14.7(8)	0.78(3) ^e
$\frac{39}{2}^+$	4016.4	630.0	11.6(9)	1.1(1) ^e
		318.2	10.3(6)	0.75(5)
$\frac{43}{2}^+$	4630.4	614.1	8.7(6)	0.9(1)
		290.4	8.0(5)	0.78(3) ^e
$\frac{47}{2}^+$	5172.6	542.3	3.3(2)	
		276.1	7.1(4)	0.75(5)
$\frac{51}{2}^+$	5802.2	629.7	3.4(3)	1.1(1) ^e
		329.5	6.0(3)	0.65(8)
$\frac{55}{2}^+$	6548.2	746.0	2.6(1)	
		388.6	2.7(1)	0.5(1)
$\frac{59}{2}^+$	7399.5	851.2	1.2(1)	
		432.9	0.7(1)	
		448.8	<0.5	

TABLE I. (*Continued.*)

I^π ^a	E_{level} (keV)	E_γ (keV) ^b	I_γ ^c	Ang.-corr. ratio
$\frac{63}{2}^+$	8328.3	928.8	0.7(1)	
$(\frac{67}{2}^+)$	(9299)	(971)	<0.5	
Band 7: [411]1/2 $\alpha = -1/2$				
$\frac{3}{2}^+$	258.0			
$\frac{7}{2}^+$	531.6	273.6	$\approx 15^f$	0.76(3)
$\frac{11}{2}^+$	909.3	377.7	14.3(7)	0.83(3)
$\frac{15}{2}^+$	1304.9	395.6	10.3(8)	0.80(3)
$\frac{19}{2}^+$	1704.3	399.4	8.1(6)	0.83(4)
$\frac{23}{2}^+$	2129.5	425.3	5.5(3)	0.76(5)
		498.1	6.0(3)	
$\frac{27}{2}^+$	2571.4	441.9	6.0(3)	0.94(5)
		466.7	5.2(3)	
$\frac{31}{2}^+$	3058.3	486.9	7.6(4)	1.09(5)
$\frac{35}{2}^+$	3597.4	539.1	4.5(3)	0.71(5)
		281.3	0.7(1)	0.78(7)
		486.0	0.5(1)	
		534.8	0.9(1)	
$\frac{39}{2}^+$	4185.6	588.2	3.9(2)	0.9(1)
$\frac{43}{2}^+$	4819.9	634.3	2.2(1)	1.1(1) ^e
$\frac{47}{2}^+$	5473.3	653.4	1.1(1)	
$\frac{51}{2}^+$	6163.8	690.5	0.7(1)	
$\frac{55}{2}^+$	6903.1	739.3	<0.5	
$\frac{59}{2}^+$	7700.7	797.6	<0.5	
$\frac{63}{2}^+$	8549.9	849.2	<0.5	
$\frac{67}{2}^+$	9453	903	<0.5	
$\frac{71}{2}^+$	10403	950	<0.5	
Band 8: [660]1/2				
$\frac{17}{2}^+$	1423.9	463.1	19(1)	0.84(4)
		238.0	19(2)	0.65(4)
		555.2	4.9(3)	0.9(1)
$\frac{21}{2}^+$	1733.0	309.1	42(3)	0.88(3)
		339.9	35(3)	0.89(2)
		406.8	12(1)	0.91(2) ^e
$\frac{25}{2}^+$	2138.7	405.7	59(6)	0.91(2) ^e
		277.0	1.0(5)	
$\frac{29}{2}^+$	2611.3	472.6	42(4)	0.94(2)
$\frac{33}{2}^+$	3140.8	529.5	35(2)	0.91(3)
$\frac{37}{2}^+$	3723.5	582.7	30(2)	0.95(4)
$\frac{41}{2}^+$	4351.7	628.2	20(1)	0.95(3)
$\frac{45}{2}^+$	4964.5	612.8	9.9(6)	1.06(3)
$\frac{49}{2}^+$	5568.0	603.5	6.2(3)	0.87(3)
$\frac{53}{2}^+$	6234.1	666.1	5.3(3)	0.91(4)
$\frac{57}{2}^+$	6950.6	716.5	1.8(1)	0.88(7)
		402.3	2.0(2)	
		791.0	1.6(1)	
$\frac{61}{2}^+$	7731.1	780.5	2.5(1)	1.2(2)
		764.4	1.3(1)	
$\frac{65}{2}^+$	8557.8	826.7	2.6(1)	
$\frac{69}{2}^+$	9447.3	889.5	1.4(1)	
$\frac{73}{2}^+$	10408.8	961.5	0.7(1)	
$\frac{77}{2}^+$	11440.5	1031.7	<0.5	
$(\frac{81}{2}^+)$	(12534)	(1093)	<0.5	
Band 9				
$\frac{25}{2}^+$	2480.7	341.9	2.2(1)	
$\frac{29}{2}^+$	2880.9	400.2	1.9(2)	1.1(1)
		269.6	2.3(2)	1.0(1)
$\frac{33}{2}^+$	3326.6	445.7	2.7(1)	0.89(7)

TABLE I. (*Continued.*)

I^π ^a	E_{level} (keV)	E_γ (keV) ^b	I_γ ^c	Ang.-corr. ratio
$\frac{37}{2}^+$	3846.8	520.2	2.1(1)	
$\frac{41}{2}^+$	4434.0	587.2	1.8(1)	0.96(8)
$\frac{45}{2}^+$	5084.4	650.4	1.1(1)	0.86(9)
		732.6	2.1(1)	
$\frac{49}{2}^+$	5795.1	710.7	1.8(2)	1.2(2)
		735.5	1.0(1)	
$\frac{53}{2}^+$	6550.9	755.8	1.3(1)	
$\frac{57}{2}^+$	7340.1	789.2	0.8(1)	
$\frac{61}{2}^+$	8174.0	833.9	<0.5	
$\frac{65}{2}^+$	9048	874	<0.5	
Band 10				
$\frac{45}{2}^+$	5059.4	707.7	3.5(4)	1.02(4) ^e
		625.3	0.5(1)	
$\frac{49}{2}^+$	5741.1	681.7	1.8(1)	0.90(8)
$\frac{53}{2}^+$	6451.4	710.3	1.6(3)	1.02(4) ^e
$\frac{57}{2}^+$	7204.6	753.2	1.4(1)	
$\frac{61}{2}^+$	8011.4	806.8	0.8(1)	
$\frac{65}{2}^+$	8879.3	867.9	0.7(1)	
$\frac{69}{2}^+$	9805.9	926.6	0.5(1)	
$\frac{73}{2}^+$	10784.0	978.1	<0.5	
$\frac{77}{2}^+$	11821	1037	<0.5	
Band 11				
$\frac{27}{2}^+$	2709.0			
$\frac{31}{2}^+$	3111.3	402.3	$\approx 1.9^f$	
$\frac{35}{2}^+$	3588.2	476.9	1.9(1)	0.71(5)
		447.1	1.0(1)	
		529.9	3.3(1)	1.1(1)
$\frac{39}{2}^+$	4134.1	545.9	4.7(2)	
		287.4	1.0(1)	
		536.5	1.1(1)	
$\frac{43}{2}^+$	4728.3	594.2	6.0(3)	
$\frac{47}{2}^+$	5361.6	633.3	4.8(2)	
$\frac{51}{2}^+$	6027.8	666.2	4.1(2)	
$\frac{55}{2}^+$	6733.5	705.7	2.9(2)	
$\frac{59}{2}^+$	7491.6	758.1	2.5(1)	
$\frac{63}{2}^+$	8311.2	819.6	1.7(1)	
$\frac{67}{2}^+$	9195.8	884.6	1.0(1)	
$\frac{71}{2}^+$	10139.1	943.3	0.5(1)	
$\frac{75}{2}^+$	11136.7	997.6	<0.5	
$\frac{79}{2}^+$	12175.6	1038.9	<0.5	
$(\frac{83}{2}^+)$	(13235)	(1059)	<0.5	
Other Levels and γ rays				
	193.2			
$\frac{31}{2}^-$	3029.3	584.5	2.4(1)	
$\frac{31}{2}^+$	3062.5	491.1	3.5(1)	
$\frac{33}{2}^+$	3316.0	253.6	0.8(1)	
		257.7	0.7(1)	

^aSpin and parity of the depopulated state.^bUncertainties in γ -ray energies are 0.2 keV for most transitions, except for relatively weak ones (<1) where 0.5-keV uncertainties are appropriate.^cRelative intensity of the γ ray with respect to the intensity of the 354.8-keV transition.^dEstimated based on intensity balance and branching ratio.^eUnresolved doublet.^fEstimated based on intensity balance.

known $E2$ transitions that are mutually coincident. The transitions coincident with these two quadrupole transitions were sorted into 16 spectra, each associated with a different ring of Gammasphere. An angular-correlation ratio was then determined by taking the intensity of a transition in the five most forward rings, $W(\theta, \phi)_{\text{for}}$, and dividing it by the intensity of the same transition in the five rings nearest 90° , $W(\theta, \phi)_{90}$. The ratio $W(\theta, \phi)_{\text{for}}/W(\theta, \phi)_{90}$ was then normalized such that known $E2$ and $E1$ transitions from neighboring nuclei had angular-correlation ratios of 1.0 and 0.6, respectively. In cases where angular-correlation ratios could not be obtained for the higher portions of a sequence, spins have been assigned to these states assuming normal rotational behavior persists throughout the band. The γ -ray and level information for ^{171}Re is given in Table I.

III. LEVEL SCHEME

The ground state of ^{171}Re has been suggested to have $(9/2^-)$ quantum numbers based on an α -decay experiment by Keller *et al.* [13] and an electron-capture decay study by Hild *et al.* [14]. In addition, both of these works provided evidence for a $(5/2^-)$ state near 190 keV. Hild *et al.* [14] also found states at 516 and 895 keV, assigning spins/parities of $(3/2^-)$ and $(7/2^-)$, respectively, and associating these with the unfavored signature of the $[541]1/2$ quasiproton configuration.

High-spin studies of ^{171}Re were previously performed by Bark *et al.* [8] and Carlsson *et al.* [9]. The former observed bands based on the $[514]9/2$, $[541]1/2$, $[402]5/2$, $[411]1/2$, and $[660]1/2$ orbitals up to spins $49/2$, $49/2$, $41/2$, $23/2$, and $41/2$, respectively. Although some of the bands were linked, the relative excitation energies were not established between all of the bands. The latter extended the structures seen by Bark *et al.* to spins $57/2$, $53/2$, $59/2$, $31/2$, and $53/2$, respectively, and found a proposed three-quasiparticle band feeding into the $[541]1/2$ sequence. More linking transitions were established between bands in this study, but none to the $[514]9/2$ structure were found. Thus, relative excitation energies were still unknown. It should be pointed out that the reported γ -ray energies between these two measurements differed by approximately 1 keV. In the present work, the calibration was thoroughly checked by ensuring that the experimental energies for the neighboring even-even nuclei $^{168,170}\text{W}$ were similar to the evaluated ones [15,16] in the ground-state sequences. Following this consistency check, it was found that the present energies generally agree with those of Ref. [8].

The level scheme of ^{171}Re resulting from this analysis is found in Figs. 1 and 2. Linking transitions were established such that all of the relative excitation energies are now known. In particular, the linking transitions between bands 1 and 2 (see Fig. 1) at high spin proved critical to link the $[514]9/2$ band to the other structures. These high-spin results greatly aid in the understanding of the nuclear structure at low spin, where the energies of the quasiproton orbitals could not be established with low-spin experimental methods. In particular, the lowest state observed is now found to be the bandhead of the $[514]9/2$ configuration, thus, supporting the decay study results for a $9/2^-$ ground state. Additionally, the $5/2^-$ state at

190 keV was confirmed and has been identified with the lowest observed level in the $[541]1/2$ sequence (band 2). The 516- and 895-keV levels were not observed, and instead the $3/2^-$ and $7/2^-$ states of the $[541]1/2$ structure were established at 301 and 448 keV, respectively. Six new decay sequences were identified in this work, and each previously known band was extended to higher spin as well.

A. Band 1

In Fig. 1, the strongly coupled sequence labeled band 1 was previously assigned as based on the $[514]9/2$ quasiproton. As discussed below, the present work is in agreement with this assignment, and the band was extended to a spin of $85/2$. Sample spectra resulting from the summation of many triple-coincidence gates in the hypercube are given in Fig. 3(a). Band 1 interacts strongly with band 2 near spin $53/2$, as seen in Fig. 1, and in the interaction region, dipole transitions are present in addition to the linking electric quadrupole transitions. The nature of the quadrupole transitions linking bands 1 and 2 was confirmed via the angular-correlation analysis with the values displayed in Table I. These results imply that bands 1 and 2 have the same parity and confirm the relative spin assignment proposed in Fig. 1.

A plot displaying the level energies minus a rigid-rotor reference for all the bands in ^{171}Re is given in Fig. 4. A near degeneracy at $53/2$ can be observed between bands 1 and 2 [Fig. 4(a)] that explains how the two interact. It is also evident that a Landau-Zener crossing [17] occurs between the $\alpha = +1/2$ signatures of bands 1 and 2; i.e., the configurations of the bands exchange character above the $53/2$ state. Thus, the $\alpha = +1/2$ sequence in band 1 becomes the favored signature of the $[541]1/2$ band above $I = 53/2$, which is why it could be extended to such high spins. In correlation to this observation, the $\alpha = +1/2$ signature of band 2 becomes the $[514]9/2$ sequence above $I = 53/2$, which explains why the dipole transitions occur between bands 1 and 2 at high spin.

B. Band 2

As stated above, the interaction between bands 1 and 2 at spin $53/2$ allows for the definitive placement of the $5/2^-$ member of band 2 at 190 keV, in accord with previous decay studies. No decay was observed from the $5/2^-$ state, even though the possible transition from this level to the $9/2^-$ ground state is allowed. As discussed in Sec. IV B, the present work assigns the $[541]1/2$ configuration to band 2, in agreement with the assignment for the $\alpha = +1/2$ sequence in Refs. [8,9]. In the $N = 96$ isotones, the $1/2^-$ bandhead of the $[541]1/2$ sequence is commonly observed below the $5/2^-$ level and the $E_\gamma(5/2^- \rightarrow 1/2^-)$ becomes systematically lower with increasing Z : ^{163}Ho $E_\gamma(5/2^- \rightarrow 1/2^-) = 29$ keV [18], ^{165}Tm 23 keV [19], ^{167}Lu 15 keV [20], and ^{169}Ta 12 keV [21]. Therefore, if the systematic trend extends to ^{171}Re , an unobserved $1/2^-$ level may exist approximately 10 keV below the $5/2^-$ state of band 2 and it would likely be isomeric. This sequence was extended from $53/2$ to $69/2$, as can be seen in the sample spectrum of Fig. 3(b), where many of the linking transitions between bands 1 and 2 can also be observed.

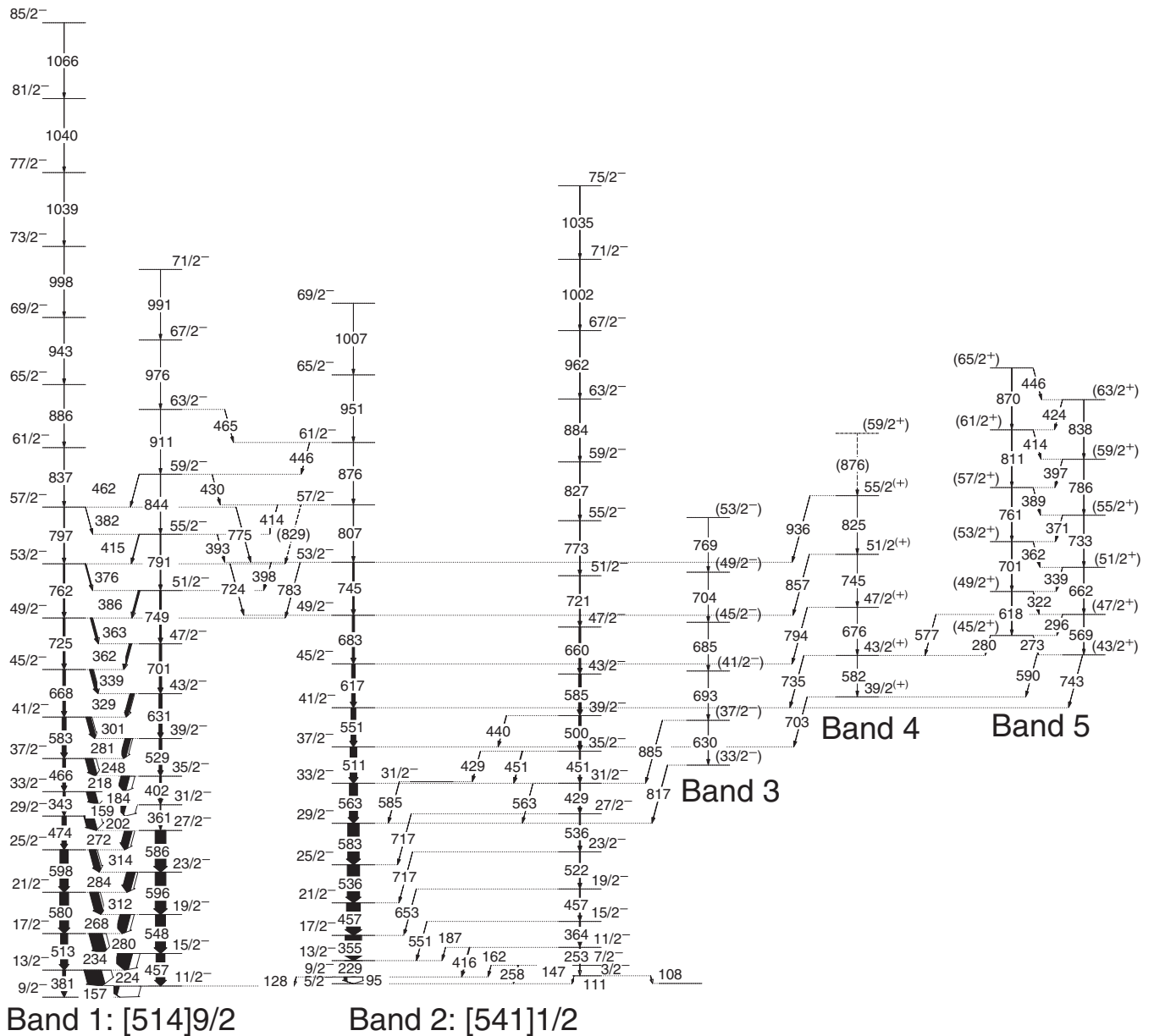


FIG. 1. Partial level scheme for ^{171}Re from the present analysis. The widths of the arrows are proportional to the relative intensities of the γ rays. Tentative levels and γ rays are indicated as dashed lines.

A portion of the $\alpha = -1/2$ signature of band 2 was previously reported by Ref. [9]; however, it was tentatively assigned a configuration involving the $h_{9/2}$ quasiproton coupled with an $i_{13/2}$ quasineutron and a negative-parity quasineutron. The linking transition reported in Ref. [9] could not be confirmed; however, a series of γ -ray transitions was found between the partners. Complexities occur in this decay sequence owing, on the one hand, to the presence of a spurious, and nearly degenerate, $31/2$ state, and on the other to the $33/2$ and $31/2$ levels having nearly identical energies in band 2. Multiple transitions with energies of 429 and 451 keV arise from this circumstance, and it was critical to have access to a hypercube in order to construct the correct decay pattern. This sequence was extended to lower spin, where many linking transitions to the $\alpha = +1/2$ member are found, as well as to higher angular

momentum reaching $75/2$. An example spectrum is given in Fig. 3(c), where the strong coincidence with the signature partner can be observed. Several of the linking transitions can be confirmed as being of $\Delta I = 1$ character from the angular-correlation analysis (see Table I). Thus, the spins of the states were firmly determined. Large signature splitting is observed in Fig. 4(a), which is common for a band associated with this high- j , low- K orbital [22].

C. Band 3

Band 3 is a new, short sequence of transitions that feeds into the $\alpha = +1/2$ signature of band 2 (see Fig. 1). The 817- and 885-keV linking transitions have angular-correlation ratios of

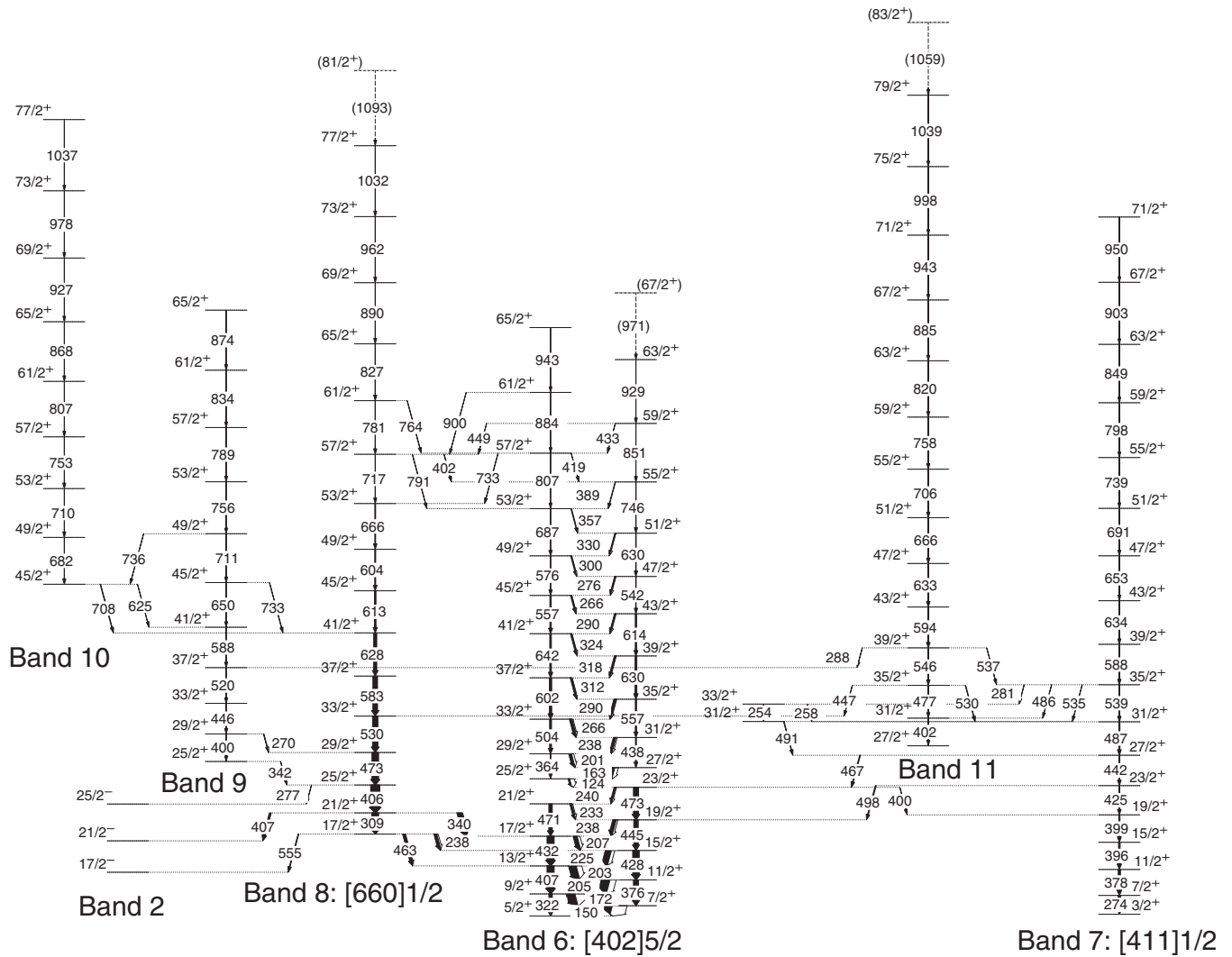


FIG. 2. Partial level scheme for ^{171}Re from the present analysis. The widths of the arrows are proportional to the relative intensities of the γ rays. Tentative levels and γ rays are given as dashed lines.

1.8(3) and 1.5(2), respectively. It has been assumed these are $E2$ in nature, however, due to the large values, it is possible that the transitions are of mixed $M1/E2$ character. The spins of band 3 must be regarded as tentative in view of this ambiguity. A spectrum of band 3, and its coincidence with band 2, is provided in Fig. 5(a). As seen in Fig. 4(a), this structure moves well above the yrast line with increasing spin, which accounts for the fact that it could not be traced to higher spin.

D. Band 4

In Fig. 1, another new, short sequence is labeled as band 4, and several linking transitions to the $\alpha = +1/2$ signature of band 2 are observed. The angular-correlation ratios of the linking transitions to band 2 are near 0.6, which is similar to the values found for known $E1$ transitions in this data set. Therefore, it has been assumed that the decay-out γ rays from band 4 are $E1$ in nature, but since it is not possible to firmly establish the nature of these transitions, the parity for band 4

has been placed in parentheses in Fig. 1. Similar to band 3, band 4 quickly moves away from the yrast line with spin, as illustrated in Fig. 4(b). One may also notice in Fig. 4(b) that the 43/2 state is nearly degenerate with levels in bands 5 and 7.

E. Band 5

Band 5 is a new, strongly-coupled structure that primarily feeds into band 4, as seen in Fig. 1. This feeding is likely a result of the two 43/2 levels being only 8 keV apart. The mixing suggests that bands 4 and 5 are of the same parity, hence positive parity is assigned to band 5. However, without further evidence (no reliable angular-correlation analysis could be performed on transitions from band 5), this assignment must be regarded as tentative. Figure 5(b) displays a sample spectrum for band 5, where the 703- and 735-keV linking transitions from band 4 to band 2 are seen, and the strong coincidence of band 5 with band 2 can be noted as well.

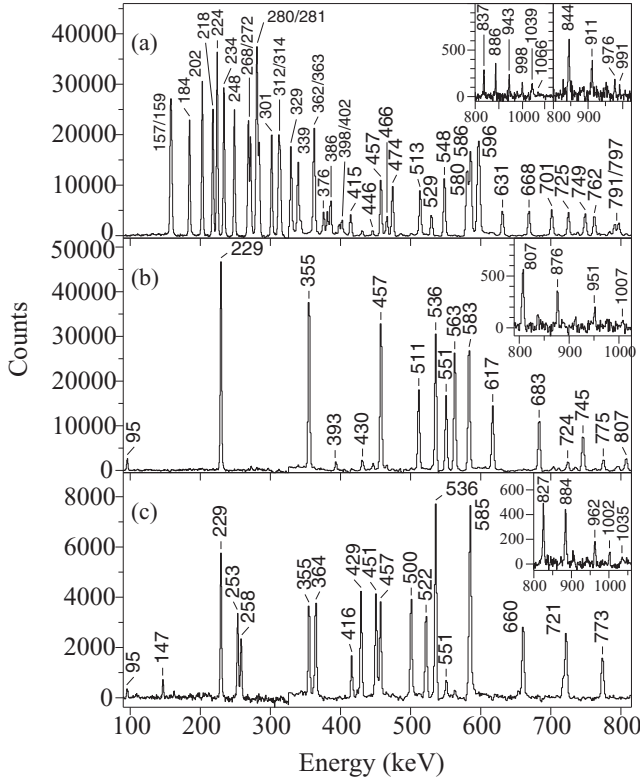


FIG. 3. (a) Spectrum for band 1 in ^{171}Re . The main spectrum results from a sum of all triple coincidence spectra between all $\Delta I = 1$ transitions in the band from the $31/2$ to the $49/2$ state. The first high-energy inset is a summation of all triple coincidence gates using a list of $E2$ transitions in the $\alpha = +1/2$ sequence from the $57/2$ to the $81/2$ state. In a similar manner, the second inset results from a list of $E2$ transitions in the $\alpha = -1/2$ structure from the $55/2$ to the $67/2$ level. (b) This spectrum for the $\alpha = +1/2$ signature of band 2 displays the transitions that are in coincidence with any two of the γ rays in the $\alpha = +1/2$ signature of band 2 between $37/2$ and $61/2$ along with a transition in the same sequence below the $33/2$ state in the same structure. The high-energy inset shows the γ rays at the top of the sequence. (c) In a similar manner to panel (b), this spectrum of the $\alpha = -1/2$ signature of band 2 is a sum of spectra where coincident transitions with any two γ rays in the $\alpha = -1/2$ signature of band 2 between spins $31/2$ and $55/2$ along with a transition in the same sequence below the $23/2$ level. The high-energy inset displays the transitions at the top of the structure.

F. Band 6

The strongly coupled sequence labeled band 6 in Fig. 2 was observed previously and assigned the $[402]5/2$ configuration. This assignment is supported by the present work (see Sec. IV F), and the spins of the levels from Refs. [8,9] were adopted. The bandhead state can now be placed at 232 keV; however, no transitions out of this level were observed. In principle, there could be a transition between the $5/2^+$ state in band 6 to the $5/2^-$ level in band 2 (located at 190 keV), but a 42-keV γ ray is below the sensitivity of the detectors in Gammasphere. Any other observed level below 232 keV would require a transition of multipolarity $M2$ or higher, which would

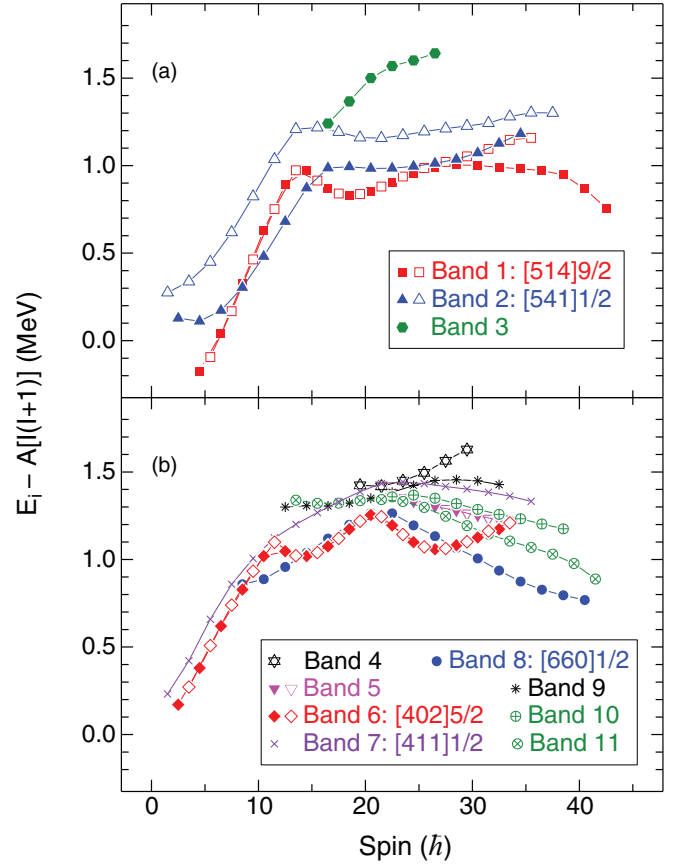


FIG. 4. (Color online) Excitation energies of the observed levels minus a rigid-rotor reference, where this reference was assumed to have a moment of inertia parameter $A = 0.007$ MeV. Positive (negative) signatures are represented with filled (open) symbols.

lead to a significant lifetime. Therefore, it is also possible that the 232-keV level is isomeric.

The $\alpha = +1/2$ signature was extended by $4\hbar$, and a slight correction was made to the $\alpha = -1/2$ signature with respect to Ref. [9]. Previously, an 827-keV line was placed above the $55/2$ level in band 6; however, from the present data, it is now clear that the 827-keV transition belongs to band 8. An 827-keV line is indeed observed in the spectrum for band 6 [Fig. 5(c)], but is a result of the coincidence between bands 6 and 8 as an interaction at $57/2$ is evident in Fig. 2. These levels are within 16 keV of each other and, apparently, mix since several linking transitions are present. It is interesting to note that two other states in bands 6 and 8 are nearly degenerate [see Fig. 4(b) and Table I]: $29/2$ (19 keV) and $41/2$ (12 keV). Despite their proximity to each other, no evidence of mixing was observed.

G. Band 7

Band 7 in Fig. 2 is a decoupled sequence that was observed in Ref. [8], but not linked, and was also reported in Ref. [9] with linking transitions into band 8. The linking transitions from Ref. [9] were not observed in the present experiment. However, several other linking transitions between bands 7 and 6, as well

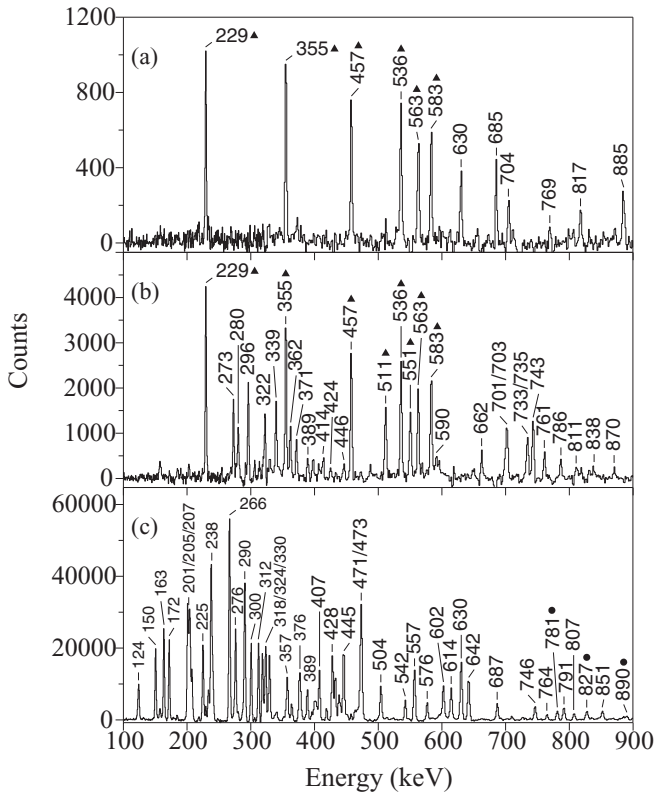


FIG. 5. (a) Spectrum for band 3 in ^{171}Re generated by summing all spectra when requiring γ rays to be in coincidence with two transitions in the $\alpha = +1/2$ sequence of band 2 (below the 29/2 level) and the 693-keV transition. (b) The summed spectrum created for band 5 displaying γ rays in coincidence with two transitions from the $\alpha = +1/2$ structure of band 2 (below the 37/2 level) and with the lowest dipole transitions in band 5. (c) Summed spectrum of all possible triple combinations in the hypercube from a list of the dipole transitions between the 25/2 and 53/2 states of band 6. Transitions denoted in the panels with filled triangles and filled circles result from bands 2 and 8, respectively.

as between bands 7 and 11, were found. These findings change the relative excitation energies from the previously reported values and band 7 can now be placed with a bandhead energy of 258 keV. Similar to band 6, no γ rays are found to depopulate the bandhead level. A 68-keV transition is possible between the $3/2^+$ state and the $5/2^-$ level of band 2, but there is no indication of such a γ ray. A 26-keV line decaying into the $5/2^+$ state of band 6 is possible, but once again, a γ ray of such low energy is not likely to be observed by the detectors in Gammasphere.

This sequence was previously observed up to the 27/2 level, and has been extended to 71/2. A spectrum is provided in Fig. 6(a). The interactions observed between bands 6 and 7 (at 23/2) and between bands 7 and 11 (at 35/2) are a result of near degeneracies that can be seen in Fig. 4(b).

H. Band 8

The decoupled structure labeled band 8 in Fig. 2 was previously identified in the prior high-spin studies [8,9]. The

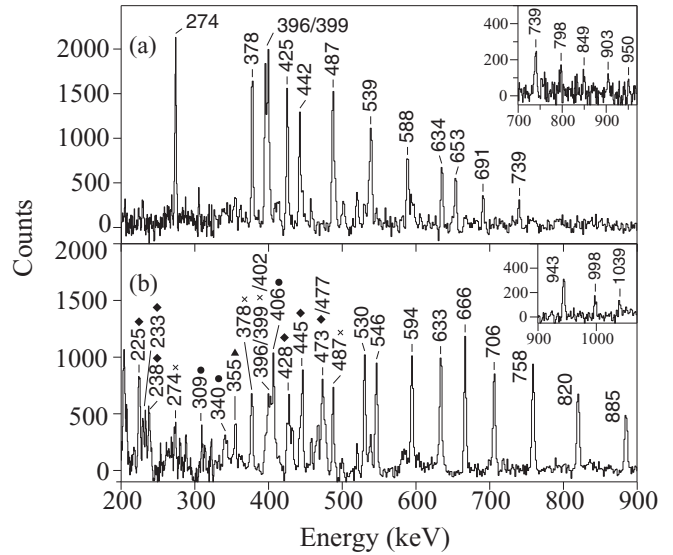


FIG. 6. (a) Spectrum for band 7 in ^{171}Re composed of the sum of the cleanest spectra resulting from a coincidence with a multitude of combinations of three in-band transitions. The inset was constructed in a similar format as the main spectrum. (b) Summed spectrum of all possible triple combinations in the hypercube from a list of transitions between the 39/2 and 79/2 states of band 11. Transitions marked with filled triangles, diamonds, crosses, and circles result from coincidences with bands 2, 6, 7, and 8, respectively.

linking transitions from band 8 into bands 2 and 6 were confirmed and the coincidence of band 8 with these two other sequences can be observed in the spectrum provided in Fig. 7(a). The angular-correlation ratio of the 238-keV line between bands 8 and 6 is consistent with a $\Delta I = 1$ dipole character. However, the angular correlations of the 340-, 463-, and 555-keV transitions are not as definite: the 340- and 463-keV lines have ratios that are near 1.0, but are low enough that an interpretation of them being dipole in nature cannot be ruled out, and the 407- and 555-keV γ rays have ratios that are consistent with $\Delta I = 0$ transitions, but once again, a clear spin assignment is difficult with these values. Fortunately, the interaction of band 8 with band 6 at 57/2 allows for a firm spin and parity assignment as the 733-keV line has an electric quadrupole nature from the angular-correlation ratio. This confirms the spins indicated in Fig. 2 for band 8 and the parity of this sequence must be the same as that of band 6. Further, Fig. 2 displays the extension of the sequence from spin 53/2 to 81/2.

I. Band 9

A new structure feeding into band 8 has been observed and is designated as band 9 in Fig. 2. Figure 7(b) displays a spectrum of band 9 and the coincidence with band 8 (as well as the subsequent decay into band 6) can be readily observed. A reliable angular-correlation ratio could not be measured for the 342-keV linking transition due to its mutual coincidence with the 340-keV line from band 8 to band 6. A ratio of 1.0(1) was determined for the 270-keV linking transition to band 8. This is consistent with an $E2$ interpretation; however, if

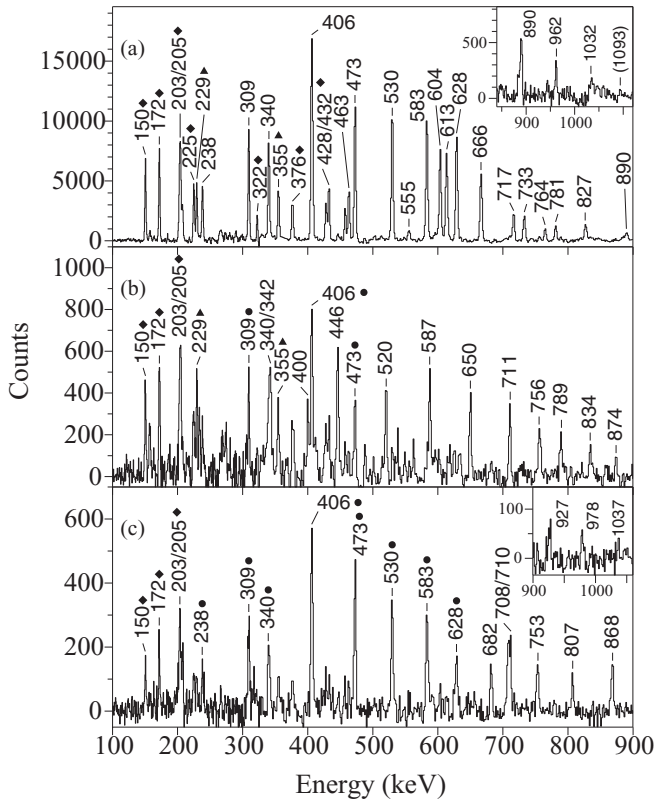


FIG. 7. (a) Transitions in band 8 resulting from a sum of spectra generated by requiring a coincidence with any two transitions in the band below the 41/2 level with a transition between the 45/2 and 77/2 states. (b) Summed spectrum of all possible triple combinations in the hypercube from a list of transitions between the 29/2 and 61/2 states of band 9. (c) Spectrum for band 10 where coincidences between all possible triple combinations of transitions from the 49/2 to the 73/2 states were summed together. For the spectra in these panels, transitions denoted with a filled triangle, filled diamond, and filled circle result from coincidences with bands 2, 6, and 8, respectively.

$\Delta I = 2$ is assumed for this transition, band 9 becomes the yrast sequence, which is not consistent with the intensity of the structure. Instead, a $\Delta I = 0$ character is preferred, which is also consistent with the angular-correlation ratio. In addition, there is an interaction between bands 9 and 10 at 45/2, requiring the levels to mix and have the same spin/parity. Based on these observations, the spins and positive parity shown for band 9 are best suited for this structure.

J. Band 10

The 45/2 level of band 10 was previously observed in Ref. [9], but no band structure was known above this level. Figure 2 shows that a sequence was extended to 77/2 based on this state, and Fig. 7(c) provides a representative spectrum for the sequence. An angular-correlation ratio of 1.02(4) was determined for the mixed 708-keV (linking) and 710-keV (inband) transitions. It is assumed that both the 708- and 710-keV lines are of $E2$ nature as the angular-correlation ratio is so close to 1.0. If one of the transitions were to be a dipole, it is likely that the measured ratio would be between

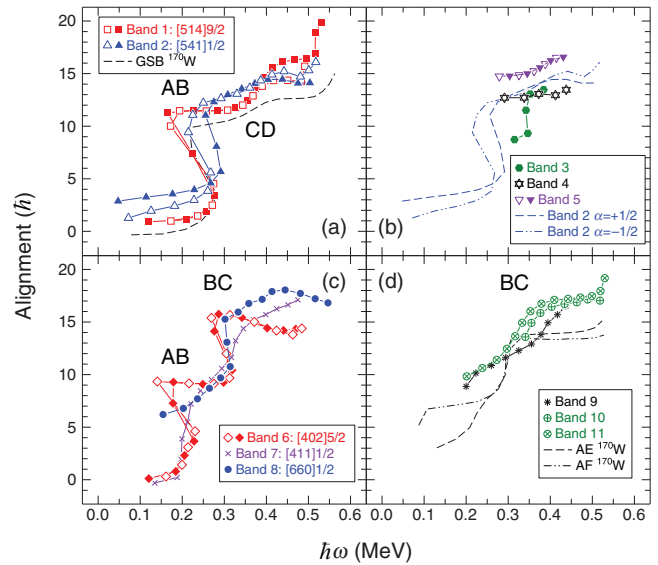


FIG. 8. (Color online) Alignments of the bands in ^{171}Re plotted vs the rotational frequency $\hbar\omega$, where Harris parameters of $\mathcal{J}_0 = 23 \hbar^2/\text{MeV}$ and $\mathcal{J}_1 = 65 \hbar^4/\text{MeV}^3$ were used for the rotation of the core. Filled (open) symbols denote the $\alpha = +1/2$ ($-1/2$) sequences. Several bands from the neighboring even-even nucleus ^{170}W are also displayed (see text for details).

0.6 and 1.0. In addition, the intensity of band 10 is consistent with the excitation energy of the structure if the spin values of Fig. 2 are adopted. Based on the assumption that the 708-keV linking transition has $E2$ character, band 10 must have the same (positive) parity as band 8. As stated above, the mixing of the 45/2 states between bands 9 and 10 then confirms that the parity of these two sequences must be the same as well.

K. Band 11

Another new decoupled structure was observed for which the decay-out pattern is divided into bands 7, 8, and 9, as seen in Fig. 2. The various low-spin γ rays can be observed in the spectrum displayed in Fig. 6(b). The complex decay pattern is largely a result of the near degeneracy of the 35/2 levels. An angular-correlation ratio of 1.1(1) (consistent with an $E2$ character) was determined for the linking, 530-keV line to band 7; thus, confirming the spin and positive parity shown in Fig. 2. As seen in Fig. 4(b), the relative energy of band 11 decreases with respect to nearly every other structure other than band 8. For this reason, band 11 could be observed up to very high spin (83/2).

IV. DISCUSSION

The rotational alignments for the 11 bands in ^{171}Re are plotted in Fig. 8, where Harris parameters of $\mathcal{J}_0 = 23 \hbar^2/\text{MeV}$ and $\mathcal{J}_1 = 65 \hbar^4/\text{MeV}^3$ were selected to subtract the angular momentum generated by the collective motion of the core. For reference, in Fig. 8(a), the alignment of the ^{170}W ground-state band (GSB) [23,24] is included, and the alignments of the two-quasineutron AE and AF bands are added in Fig. 8(d).

TABLE II. Parameters used in calculating theoretical $B(M1)/B(E2)$ values shown in Fig. 10.

Configuration	$g\Omega$	$i_x (\hbar)$
$\pi h_{11/2}[514]9/2$	1.30	1.0
$\pi d_{5/2}[402]5/2$	1.57	0.0
$\nu i_{13/2} AB$	-0.27	10.5
$\nu i_{13/2} BC$	-0.27	6.5
$\nu i_{13/2} A$	-0.27	5.2
$\nu h_{9/2} E, F$	-0.35	1.0

The quasiparticle labeling scheme is summarized in Table II. The observed crossings seen in Fig. 8 were interpreted with the calculations of the cranked shell model (CSM) [25], presented in Fig. 9. A quadrupole deformation parameter of $\beta_2 = 0.209$ was used from the prediction in Ref. [26], and $\gamma = 0^\circ$ was assumed. Pairing energies of $\Delta_p = \Delta_n = 1.26$ MeV were calculated using the five-point mass fit discussed in Ref. [27]. Crossings are indicated in Fig. 9 using the same labeling convention given in Table II.

Three strongly coupled structures were observed in ^{171}Re ; and the $B(M1)/B(E2)$ ratios were determined for bands 1, 5, and 6 as a result. Figure 10 presents these ratios along with calculated ones based on the geometrical approximation for

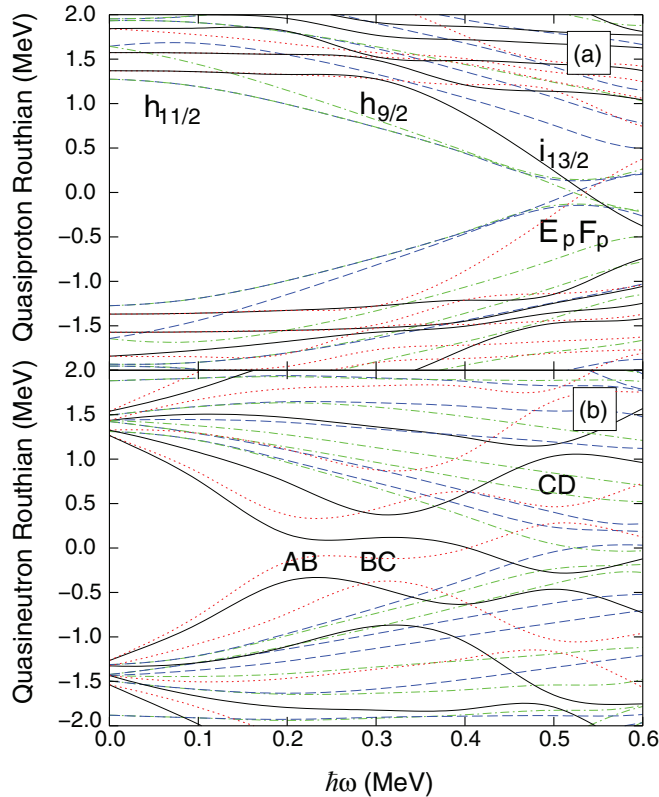


FIG. 9. (Color online) Quasiparticle Routhian energies for ^{171}Re from the cranked shell model. A quadrupole deformation of $\beta_2 = 0.209$ and pairing energies of $\Delta_p = \Delta_n = 1.26$ MeV were assumed. The solid (dotted) lines represent positive parity and $\alpha = +1/2$ ($\alpha = -1/2$) Routhians, while the dashed (dash-dotted) lines represent negative parity with $\alpha = -1/2$ ($\alpha = +1/2$) Routhians.

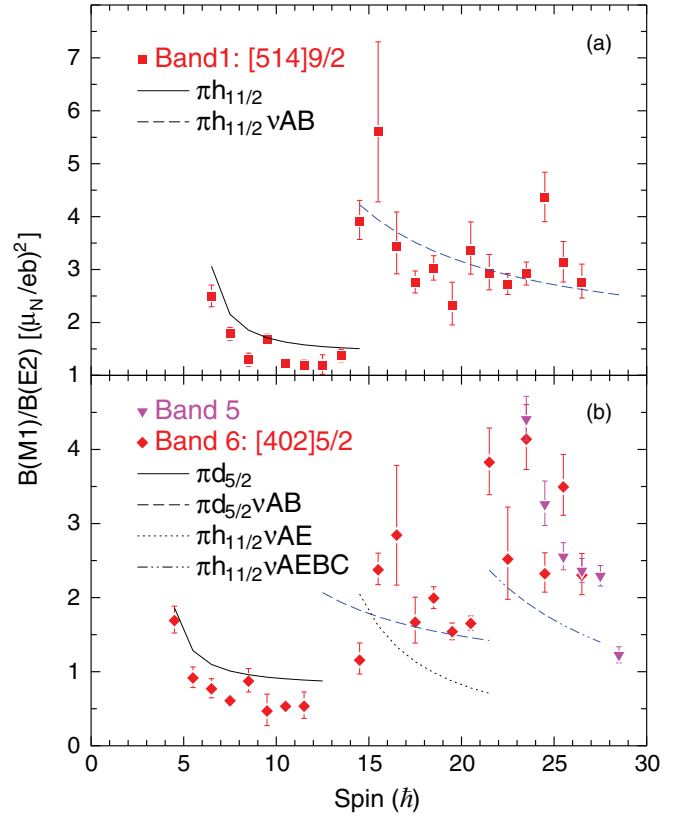


FIG. 10. (Color online) $B(M1)/B(E2)$ ratios for the strongly coupled sequences in ^{171}Re . Calculations of the theoretical values are described in the text and the parameters used are listed in Table II.

$B(M1)$ strength [28] and the rotational form of the $B(E2)$ strength [29]. A quadrupole moment of $5.66 e b$ was assumed, based on the predicted deformation from above. The collective gyromagnetic parameter was set at $g_R = Z/A = 0.439$ and the $g\Omega$ and i_x parameters displayed in Table II were used as input to the $B(M1)/B(E2)$ theoretical calculations.

A. Band 1

This strongly coupled sequence was previously assigned the $\pi h_{11/2}[514]9/2$ configuration [8,9], and, indeed, the initial alignment of $\sim 1 \hbar$ seen in Fig. 8(a) is consistent with this interpretation. In addition, the experimental and theoretical $B(M1)/B(E2)$ ratios agree with this configuration, although the theoretical values are slightly higher [see Fig. 10(a)]. This may indicate that the quadrupole moment is somewhat higher than that assumed in the calculations. Both signatures of this structure undergo a backbend where the crossing frequency is determined to be 0.23 MeV, in agreement with the CSM prediction for the AB crossing in Fig. 9(b).

At higher frequencies, another gain in alignment is seen near 0.38 MeV, that is similar in behavior to that displayed by the GSB of ^{170}W . In Ref. [23], it was suggested that this crossing in ^{170}W was the result of two $h_{11/2}$ quasiprotons aligning. However, such a crossing would be Pauli blocked in the $[514]9/2$ band in ^{171}Re . The absence of blocking suggests

that a different interpretation is required. In the sequences where the BC crossing is observed, no such alignment is seen near 0.38 MeV (see Sec. IV F). Thus, it is likely that the crossing at 0.38 MeV involves the C quasineutron, and the CD alignment is assigned to this alignment gain. The inspection of Fig. 9(b) suggests that the CD crossing occurs at a lower frequency than the CSM predicts. It is possible that the AB alignment reduces the neutron pairing field which in turn would lower the predicted CD crossing frequency.

It may be observed in Fig. 8(a) that the $\alpha = +1/2$ sequence gains approximately $2\hbar$ more alignment than its signature partner above 0.4 MeV. This is the result of the Landau-Zener crossing, discussed above, where the $\alpha = +1/2$ structure changes from being predominantly of $\pi h_{11/2}$ character to $\pi h_{9/2}$ parentage. In fact, near 0.4 MeV, the $\alpha = +1/2$ sequence from band 2 has the same amount of alignment as the $\alpha = -1/2$ signature of band 1 and this is consistent with a change of configuration. Such an interaction is reproduced well by the CSM, as seen in Fig. 9(a), where the Routhians of the $\pi h_{11/2}$ and $\pi h_{9/2}$ mix just above 0.4 MeV.

At the highest frequencies, a third crossing is observed above 0.5 MeV in the $\alpha = +1/2$ sequence. This may correspond with the $h_{11/2}$ quasiproton crossing ($E_p F_p$), since this sequence has changed its character to a $\pi h_{9/2}$ parentage and would not block such an alignment. In addition, the CSM predicts that this quasiproton crossing would occur near this frequency [Fig. 9(a)].

B. Band 2

Previously, the $\alpha = +1/2$ signature of band 2 was assigned the $h_{9/2}[541]1/2$ configuration [8,9], while the $\alpha = -1/2$ signature was tentatively assigned the $\pi h_{9/2}\nu AF$ configuration. With the present observation of this latter signature down to lower spins, the two sequences can be confidently interpreted as signature partners of the $[541]1/2$ orbital. The alignments for band 2 are displayed in Fig. 8(a) where the $\alpha = +1/2$ signature has an initial alignment of $\sim 3\hbar$ and the AB crossing is found to be delayed ($\hbar\omega_c = 0.28$ MeV) with respect to the GSB in the neighboring even-even nucleus. Both characteristics are in accordance with other known $[541]1/2$ bands [22]. The $\alpha = -1/2$ signature has an initial alignment approximately $1\hbar$ less than its partner, typical for the unfavored partner of high- j , low- K bands. Its AB crossing frequency is delayed less as it occurs at 0.24 MeV. Following the AB crossing, both signatures gradually gain an alignment that may be associated with the CD crossing. At the highest frequencies in the $\alpha = -1/2$ sequence, there is the apparent beginning of a crossing near the same frequency as that seen in $\alpha = +1/2$ signature of band 1, and this observation may be attributed to the $h_{11/2}$ quasiproton crossing as well.

C. Band 3

Not much information is available to assist with the assignment for band 3. However, as can be seen in Fig. 8(b), the band appears to be in the middle of a crossing near 0.35 MeV. It is possible that this is associated with either the BC or AD crossings, but it is proposed instead that band

3 is the continuation of the $[541]1/2$ band that undergoes the $BCAD$ alignment, similar to ground-state bands in the nearby even-even nuclei. This assignment must be regarded as tentative in view of the limited data available.

D. Band 4

Similar to band 3, it is difficult to propose a configuration for band 4 on the basis of the available information. If the assumption that a series of electric dipole transitions feed the $[541]1/2$ sequence (band 2) is correct, it may suggest the presence of octupole correlations. However, it is not typical for octupole vibrations to be found at higher energies and spins in nuclei of this mass region. In addition, under the hypothesis of an octupole phonon coupled to the $[541]1/2$ configuration, one would observe a higher alignment in the vibrational sequence in comparison with the band on which it is based. In Fig. 8(b), band 4 has nearly the same (or slightly lower) alignment as the $[541]1/2$ structure over the region for which it is seen, and an octupole vibration interpretation does not seem plausible. Another possible interpretation for band 4 would be that it is based on a low- K , positive-parity quasiproton above the AB crossing, since only one signature is found. The sequence associated with the $d_{3/2}$ quasiproton has been previously identified [8,9] (band 7), and band 4 has the same signature as this band; therefore, it cannot be the signature partner of this configuration either. It is possible that band 4 is the unfavored signature of the $i_{13/2}$ configuration (band 8); however, this is highly unlikely as its alignment value is significantly less than that found for band 8 in Fig. 8(c). Hence, it is not possible to propose a configuration for this sequence at this time.

E. Band 5

Considering that band 5 is observed at relatively high energy (>4800 keV), it is likely to be associated with a five-quasiparticle configuration. As discussed in Sec. III E, this sequence may have positive parity, and since it is strongly coupled, at least one of the quasiparticles should have a high- K value. The experimental $B(M1)/B(E2)$ ratios for band 5 are presented in Fig. 10(b), where they are seen to be similar to those of band 6 in the same spin range. The configuration for band 6 in this region is proposed to be $\pi h_{11/2}\nu AEBC$ (see Sec. IV F); therefore, it is possible that band 5 is its signature partner $\pi h_{11/2}\nu AFBC$. The alignment values for bands 5 and 6 [see Figs. 8(b) and 8(c), respectively] are similar in the 0.3–0.5-MeV frequency region. However, their trajectories are different, in that the alignment of band 5 increases with frequency while the alignment of band 6 decreases. Thus, the proposed $\pi h_{11/2}\nu AFBC$ configuration for band 5 remains tentative.

F. Band 6

Band 6 was previously proposed as based on the $d_{5/2}[402]5/2$ configuration in Refs. [8,9]. The nearly zero initial alignment [Fig. 8(c)] is consistent with this assignment, as is the agreement between experimental and theoretical

$B(M1)/B(E2)$ ratios for spins below $25/2$ [Fig. 10(b)]. Thus, the $[402]5/2$ interpretation is adopted here as well. One may observe in Fig. 8(c) that the alignment gain at low frequency (~ 0.2 MeV) is not as smooth as that in bands 1 and 2. References [8,9] give an explanation for this phenomenon based on a crossing with a more deformed band with the same $d_{5/2}$ configuration, but whose core is at a higher deformation due to the occupation of a pair of quasiprotons in the $h_{9/2}$ orbital.

The AB crossing is clearly observed at 0.20 MeV, slightly below the CSM prediction of 0.23 MeV. A second crossing is present at 0.30 MeV, in agreement with the BC crossing frequency [Fig. 9(b)]. This BC crossing would be blocked in band 6 if it remained associated with the $\pi d_{5/2}\nu AB$ configuration. However, as seen in other nearby nuclei [30–32], it is likely that band 6 exchanges character and becomes the $\pi h_{11/2}\nu AE$ configuration instead. Indeed, this sequence was recently identified in ^{169}Re [33]. With this interpretation, the BC crossing is allowed. The $B(M1)/B(E2)$ ratios are compared with the $\pi d_{5/2}\nu AB$ and $\pi h_{11/2}\nu AE$ configurations in Fig. 10(b). Either configuration describes the experimental data; therefore, it is possible that there is significant mixing in the sequence between spins $29/2$ and $41/2$. Following the BC crossing, the experimental $B(M1)/B(E2)$ ratios are in best agreement with the $\pi h_{11/2}\nu AEBC$ configuration.

G. Band 7

The alignment plot for band 7 is complex as delineated in Fig. 8(c). Its initial value is near zero, but begins to gain alignment almost immediately. Once again, Ref. [9] suggests that this behavior through the AB crossing region corresponds to interaction with a more deformed band. This sequence was previously identified as being based on the $d_{3/2}[411]1/2$ configuration, and is adopted here as well. However, band 7 continues to gain alignment throughout the observed frequency range. If a configuration change occurs (similar to that observed in band 6), it is possible that some of the alignment gain is a result of either the BC or AD crossing. Another possible scenario is that band 7 is crossed by the unfavored signature of the $\pi i_{13/2}\nu AB$ sequence. This would increase the alignment to values similar to those of band 8, which has been interpreted as the $i_{13/2}$ sequence (see below). However, these scenarios remain conjectures at this point.

H. Band 8

An initial alignment of nearly $6\hbar$ is observed for band 8 in Fig. 8(c). This is a strong indication for a high- j , low- K sequence. The previous high-spin studies [8,9] associated this band with the $i_{13/2}[660]1/2$ configuration. This configuration is assigned here as well, as the expected initial alignment would be $\sim 6\hbar$ and the AB crossing would be significantly delayed due to the large amount of deformation usually associated with this intruder orbital. Indeed, the first crossing is observed at 0.31 MeV, interpreted as the AB crossing even though it occurs at the same frequency as the predicted BC alignment. The discontinuity in the alignment plot near 0.35 MeV [Fig. 8(c)] is caused by the interaction with band 6. This mixing of

states allows one to estimate the relative quadrupole moments between the bands and this point is discussed in Sec. V. In addition, a search for a wobbling sequence based upon this structure was performed, and this is discussed in Sec. V as well, in view of the fact that all known wobbling bands in this region are based on the $\pi i_{13/2}$ structure.

I. Bands 9, 10, and 11

The decoupled sequences labeled as bands 9, 10, and 11 in Fig. 2 are all likely of positive parity. In addition, the lowest states are observed in an energy range where three-quasiparticle structures are most likely to occur. Inspection of the lower-spin portion of these bands ($I = 25/2$ – $43/2$) in Fig. 4(b), as well as of the lower frequency region (0.2–0.3 MeV) of their alignment plots in Fig. 8(d), indicates that bands 9 and 11 behave as signature partners. The alignments for the AE and AF configurations from ^{170}W have also been plotted in Fig. 8(d) for reference. Bands 9 and 11 can be seen to have approximately $3\hbar$ more alignment than the AF configuration for the lower frequency region (the structure labeled as AE is likely the octupole vibrational structure at these frequencies). This difference is identical with the amount of alignment associated with the favored signature of the $\pi h_{9/2}[541]1/2$ sequence, as displayed in Fig. 8(a). Therefore, the $\pi h_{9/2}\nu AE$ and $\pi h_{9/2}\nu AF$ configurations are proposed for bands 11 and 9, respectively, at the lower spins.

Above this spin/frequency region, bands 9 and 11 deviate from each other, as can be observed in both Figs. 4(b) and 8(d). However, the alignment values for band 10 clearly track with those of band 11 above 0.3 MeV [Fig. 8(d)]. Both bands 10 and 11 experience a crossing at 0.33 MeV that is somewhat delayed from the BC crossing at 0.3 MeV in band 6 and the AE/AF bands of ^{170}W . Assuming that the crossing in bands 10 and 11 are of BC origin, the delay is consistent with the presence of an $h_{9/2}$ quasiproton in their configurations. As stated previously in Sec. IV B, this quasiproton likely drives the nucleus to a larger deformation, that delays observed crossings. Thus, bands 10 and 11 are assigned the $\pi h_{9/2}\nu AFBC$ and $\pi h_{9/2}\nu AEBC$ configurations above 0.33 MeV. Above 0.4 MeV, band 11 has slightly more alignment than band 10, consistent with the slight difference between the AE and AF configurations in ^{170}W following the BC alignment, see Fig. 8(d).

The configuration of band 9 above 0.3 MeV is not clear. Perhaps it represents the continuation of the $\pi h_{9/2}\nu AF$ structure that is bypassing the BC crossing. The alignment gain near 0.38 MeV may then be interpreted as the CD crossing. However, this assignment must be considered as tentative at this point.

V. SEARCH FOR WOBBLING AND POSSIBLE EVOLUTION OF DEFORMATION IN THE $\pi i_{13/2}$ SEQUENCE

The primary motivation for investigating high-spin states in ^{171}Re was the evidence for the wobbling mode in nearby tantalum and lutetium nuclei. The key characteristics of wobbling sequences in this region are that they feed the

$\pi i_{13/2}$ structure and share similar properties (e.g., dynamic moment of inertia, alignment, and quadrupole moment) with this $\pi i_{13/2}$ excitation. Two states were previously observed feeding into the $\pi i_{13/2}$ band in Ref. [9]. Therefore, these were first investigated in connection with a wobbling sequence. As a result, band 10 was identified, but, its alignment and dynamic moment of inertia do not resemble those of the $\pi i_{13/2}$ structure and it cannot be considered as a candidate for wobbling.

The fact that the dynamic moments of inertia are dependent on the spacings of successive γ rays allows for a search to be performed with lists of gating transitions having spacings similar to those characteristic of the $\pi i_{13/2}$ band. This sequence undergoes a backbend which dictated separate searches below and above the backbend. Summed spectra from a coincidence hypercube, generated by lists of five γ -ray energies, were inspected. Each γ -ray energy in the list was subsequently changed by 1 keV (with spacings identical to, or slightly different from those in the $i_{13/2}$ band) to form new spectra. This search procedure was carried out through a region of hundreds of keV. Unfortunately, no signal of a wobbling structure was identified. An upper limit for such a sequence (if one exists) would be 1% of the intensity of the 354.8-keV line in band 2, since the weakest sequence (band 5) was observed at this level. Note that the $\pi i_{13/2}$ sequence (band 8) was observed with a maximum yield of 59%. Thus, the upper limit on a ^{171}Re wobbling band is much weaker than the 10–25% levels (with respect to the $\pi i_{13/2}$ structure) at which it has been observed in other nuclei.

A possible clue as to why wobbling was not observed in ^{171}Re may be inferred from the interaction between the $\pi i_{13/2}$ structure and band 6 at spin 57/2 (Fig. 2). The mixing of the 57/2 states in these two bands allows one to estimate the ratio of the associated quadrupole moments, assuming pure two-state mixing. A mixing amplitude α between the normal (ND) and proposed strongly deformed (SD) states can be determined from the $B(E2)_{\text{inter}}/B(E2)_{\text{intra}}$ ratio using the transitions depopulating the 61/2 level by the equation [34]:

$$\frac{B(E2 : 764.4)}{B(E2 : 780.5)} = \frac{\alpha^2}{1 - \alpha^2} = \frac{I_\gamma(764.4)}{I_\gamma(780.5)} \left(\frac{780.5}{764.4} \right)^5. \quad (1)$$

The intensities of Table I lead to a value of the ratio $\alpha^2/(1 - \alpha^2) = 0.58(7)$. A ratio for the quadrupole moments of the bands can then be calculated with the $B(E2)_{\text{inter}}/B(E2)_{\text{intra}}$ ratio from the 57/2 level as

$$\begin{aligned} \frac{B(E2 : 791.0)}{B(E2 : 716.5)} &= \frac{\alpha^2}{1 - \alpha^2} \frac{Q_{ND}^2 \langle I_i K_{ND} 20 | I_f K_{ND} \rangle^2}{Q_{SD}^2 \langle I_i K_{SD} 20 | I_f K_{SD} \rangle^2} \\ &= \frac{I_\gamma(716.5)}{I_\gamma(791.0)} \left(\frac{716.5}{791.0} \right)^5, \end{aligned} \quad (2)$$

where $K_{ND} = 5/2$ and $K_{SD} = 1/2$. The resulting quadrupole moment ratio is then $Q_{SD}/Q_{ND} = 1.0(1)$, suggesting that the $\pi i_{13/2}$ sequence (above the AB crossing) has nearly the same deformation as band 6.

This result is somewhat surprising as the $i_{13/2}$ quasiproton is well known for driving the nucleus to higher deformations. In fact, a similar analysis of the $\pi i_{13/2}$ band interacting with a normal deformed band in ^{171}Ta gave a ratio of

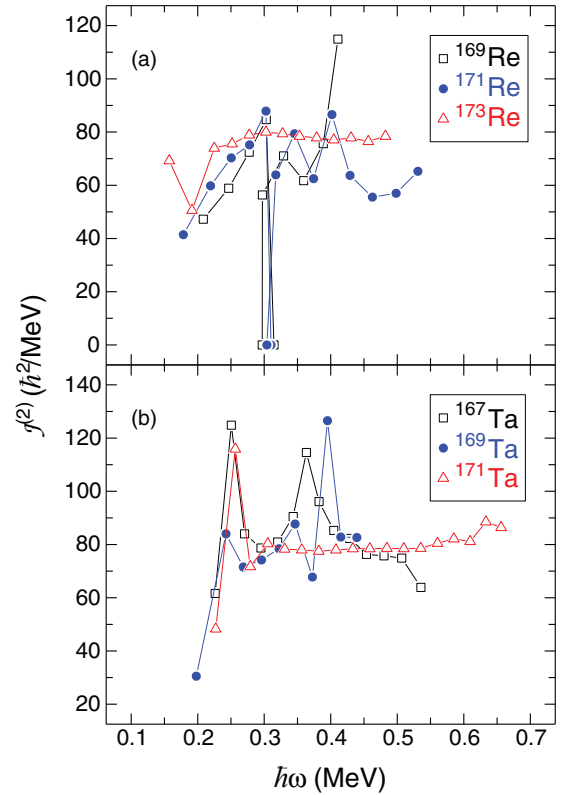


FIG. 11. (Color online) Dynamic moments of inertia for the $\pi i_{13/2}$ bands in (a) $^{169,171,173}\text{Re}$ and (b) $^{167,169,171}\text{Ta}$.

$Q_{SD}/Q_{ND} = 1.67(24)$ confirming the enhanced deformation of the $\pi i_{13/2}$ structure in this isotope [32]. In addition, the fact that the AB crossing in the ^{171}Re sequence is found to be significantly delayed strongly implies a larger deformation than the one associated with the other bands in this nucleus. Therefore, other factors were considered in order to develop a better understanding of what may be occurring above the AB crossing in the $\pi i_{13/2}$ band.

Dynamic moments of inertia are often correlated with deformation and these are presented as a function of frequency in Fig. 11 for the $\pi i_{13/2}$ bands in $^{169,171,173}\text{Re}$ and in $^{167,169,171}\text{Ta}$. One may note that the $N = 98$ nuclei (^{171}Ta and ^{173}Re) display a nearly constant moment of $\sim 80 \hbar^2/\text{MeV}$ above $\hbar\omega = 0.3$ MeV. The quadrupole moment for this $i_{13/2}$ band was measured in ^{173}Re [35] and was reported to be “considerably larger than the $h_{9/2}$ band,” making it a good reference for the other structures. As seen in Fig. 11(b), the $i_{13/2}$ sequences in the lighter tantalum nuclei have moments near $80 \hbar^2/\text{MeV}$, suggesting deformations similar to the $N = 98$ cases, and a wobbling band was observed in ^{167}Ta [5,6]. However, above 0.3 MeV (where the AB crossing occurs) in ^{171}Re , the dynamic moment of inertia of this structure is significantly less than that found in ^{173}Re . A smaller dynamic moment of inertia implies a smaller deformation and this may be viewed as another indication that the deformation may not be large above the AB crossing.

Finally, by inspecting Fig. 4(b), one finds two other spin values where bands 6 and 8 are nearly degenerate. At 57/2, the energy separation between levels is 16 keV, while at 29/2

and 41/2 differences of 19 and 12 keV are found, respectively. If a strong interaction is found at 57/2 between the bands, the question arises about why there is no evidence of mixing between the two lower spin states. In particular mixing would be anticipated with the 41/2 levels being so close in energy. Perhaps, the answer is related to a significant deformation difference between the bands at 29/2 and 41/2 (both below or in the AB crossing region, respectively), while the bands have similar deformation at higher spins leading to the interaction at 57/2.

The quadrupole moment ratio, dynamic moment of inertia difference, and lack of mixing at lower spins are all indirect indications of a possible lower deformation in the $i_{13/2}$ sequence at higher spins in ^{171}Re . Only a lifetime measurement will validate this hypothesis of a deformation change at high spin. However, if this $\pi i_{13/2}$ structure is not strongly deformed ($\beta_2 \approx 0.35$), the energy gap at the triaxial deformation parameter $\gamma \approx 20^\circ$ described in Ref. [7] will not occur, and an asymmetric shape is not likely to stabilize.

VI. SUMMARY

High-spin states were populated in the $N = 96$ nucleus ^{171}Re in order to investigate the role of the quasiproton Fermi surface in the observation of the exotic wobbling mode. All of the previously known rotational sequences were extended to higher spin and six new structures were observed. Of particular interest, the $\pi i_{13/2}$ band (on which all known wobbling bands in this region are based) was extended to spin 81/2, but no

evidence for the mode was found. An interaction between the $i_{13/2}$ structure (which is typically known to enhance the deformation) and a normal deformed band suggests that the former may not be significantly deformed at higher spins. Supporting evidence was found in the fact that the dynamic moment of inertia of the $i_{13/2}$ sequence in ^{171}Re is lower than that found in the same band of ^{173}Re (where lifetime measurements indicate it is strongly deformed). If the $i_{13/2}$ band in ^{171}Re is indeed not highly deformed at high spin, this would perhaps explain why no wobbling was observed as the stable triaxial deformation is dependent on a large quadrupole deformation. A lifetime measurement is required in order to verify the onset of lower deformation at high spin in the ^{171}Re $i_{13/2}$ structure.

ACKNOWLEDGMENTS

The authors thank the ANL operations staff at Gammasphere and gratefully acknowledge the efforts of J. P. Greene for target preparation. We thank D. C. Radford and H. Q. Jin for their software support. This work was funded by the National Science Foundation under Grants No. PHY-1203100 (USNA), No. PHY-0754674 (FSU), and No. PHY-1068192 (ND), the U.S. Department of Energy, Office of Nuclear Physics, under Contracts No. DE-AC02-06CH11357 (ANL), No. DE-FG02-94ER40848 (UML), No. DE-FG02-96ER40983 (UT), No. DE-FG02-94ER40834 (UMCP), and No. DE-FG02-95ER40939 (MSU), as well as the United Kingdom Science and Technology Facilities Council.

-
- [1] S. W. Ødegård *et al.*, *Phys. Rev. Lett.* **86**, 5866 (2001).
 [2] G. Schönwaßer *et al.*, *Phys. Lett. B* **552**, 9 (2003).
 [3] H. Amro *et al.*, *Phys. Lett. B* **553**, 197 (2003).
 [4] P. Bringel *et al.*, *Eur. Phys. J. A* **24**, 167 (2005).
 [5] D. J. Hartley *et al.*, *Phys. Rev. C* **80**, 041304(R) (2009).
 [6] D. J. Hartley *et al.*, *Phys. Rev. C* **83**, 064307 (2011).
 [7] H. Schnack-Petersen *et al.*, *Nucl. Phys. A* **594**, 175 (1995).
 [8] R. A. Bark, G. D. Dracoulis, A. E. Stuchbery, A. P. Byrne, A. M. Baxter, F. Riess, and P. K. Weng, *Nucl. Phys. A* **501**, 157 (1989).
 [9] H. Carlsson *et al.*, *Nucl. Phys. A* **551**, 295 (1993).
 [10] R. V. F. Janssens and F. S. Stephens, *Nucl. Phys. News* **6**, 9 (1996).
 [11] M. Cromaz *et al.*, *Nucl. Instrum. Methods Phys. Res., Sect. A* **462**, 519 (2001).
 [12] D. C. Radford, *Nucl. Instrum. Methods Phys. Res., Sect. A* **361**, 297 (1995).
 [13] J. G. Keller, K.-H. Schmidt, F. P. Hessberger, G. Münzenberg, W. Reisdorf, H.-G. Clerc, and C.-C. Sahn, *Nucl. Phys. A* **452**, 173 (1986).
 [14] T. Hild, W.-D. Schmidt-Ott, V. Kunze, F. Meissner, C. Wennemann, and H. Grawe, *Phys. Rev. C* **51**, 1736 (1995).
 [15] C. M. Baglin, *Nucl. Data Sheets* **111**, 1807 (2010).
 [16] C. M. Baglin, *Nucl. Data Sheets* **96**, 611 (2002).
 [17] L. D. Landau, *Phys. Z. Sowjetunion* **2**, 46 (1932); C. Zener, *Proc. R. Soc. London A* **137**, 696 (1932).
 [18] B. Singh and A. R. Farhan, *Nucl. Data Sheets* **89**, 1 (2000).
 [19] A. K. Jain, A. Ghosh, and B. Singh, *Nucl. Data Sheets* **107**, 1075 (2006).
 [20] D. Barnéoud and C. Foin, *Nucl. Phys. A* **287**, 77 (1977).
 [21] D. J. Hartley *et al.*, *Phys. Rev. C* **74**, 054314 (2006).
 [22] H. J. Jensen *et al.*, *Nucl. Phys. A* **695**, 3 (2001).
 [23] J. Recht *et al.*, *Nucl. Phys. A* **440**, 366 (1985).
 [24] S. Miller *et al.* (unpublished).
 [25] R. Bengtsson and S. Frauendorf, *Nucl. Phys. A* **314**, 27 (1979); **327**, 139 (1979).
 [26] P. Möller, J. R. Nix, W. D. Myers, and W. J. Swiatecki, *At. Data Nucl. Data Tables* **59**, 185 (1995).
 [27] S. K. Tandel *et al.*, *Phys. Rev. C* **77**, 024313 (2008).
 [28] F. Döna, *Nucl. Phys. A* **471**, 469 (1987).
 [29] A. Bohr and B. R. Mottelson, *Nuclear Structure* (Benjamin, New York, 1975), Vol. II.
 [30] D. R. Jensen *et al.*, *Nucl. Phys. A* **703**, 3 (2002).
 [31] G. Schönwaßer *et al.*, *Nucl. Phys. A* **735**, 393 (2004).
 [32] D. J. Hartley *et al.*, *Phys. Rev. C* **72**, 064325 (2005).
 [33] D. J. Hartley *et al.*, *Phys. Rev. C* **87**, 024315 (2013).
 [34] J. Domscheit *et al.*, *Nucl. Phys. A* **660**, 381 (1999).
 [35] N. R. Johnson *et al.*, *Phys. Rev. C* **55**, 652 (1997).